Prescission and postscission neutrons from the reactions $p + ^{235,236,238}U$ with $E_p \leq 25.6$ MeV

M. Strecker, R. Wien, P. Plischke,* and W. Scobel
I. Institut für Experimentalphysik, Universität Hamburg, D-2000 Hamburg 50, Federal Republic of Germany
(Received 11 September 1989)

Prescission (ν_{iso}) and postscission (ν_{post}) neutron multiplicities have been measured for the reactions $p + ^{235,236,238}U$ at several projectile energies between 12.7 and 25.6 MeV in coincidence with binary fragments. Separation of ν_{iso} from ν_{post} was achieved under the assumption of isotropic emission in the respective source frames. Both multiplicities increase with initial excitation energy E^*_{CN} with comparable rates $\Delta E^*_{CN}/\Delta\nu \approx 17 \pm 3$ MeV. $\nu_{iso}(E^*_{CN})$ extends existing data of heavy-ion induced fusion-fission with $E^*_{CN} \geq 50$ MeV; for $E^*_{CN} \geq 20$ MeV it is incompatible with the transition-state model and cannot be reproduced without a delay time for the fission competition in the order of $3\times10^{-20}-10^{-19}$ s. The fragment mass dependence $\nu_{post}(m)$ shows a clear sawtooth structure for all three targets at $E_p = 12.6$ MeV that is gradually washed out with increasing E_p or decreasing total kinetic energy TKE, because the heavier fragment receives most of the additional excitation energy. The nuclear temperatures of the heavy fragments exceed those of the light ones, but seem to approach each other with increasing fragment excitation.

I. INTRODUCTION

The measurement of fusion-fission coincident neutrons provides access to the time scale on which the emission of light particles precedes or competes with a fragmentation of the reaction system.[1,2]

The onset of the reaction is characterized by preequilibrium emission. It is followed by a cascade of neutrons evaporated from an equilibrated composite system. Both categories are referred to as prescission neutrons with the multiplicities ν_{iso}. When the system approaches the scission point, a third generation of neutrons is contributed from the nascent, accelerating or fully accelerated fragments. The multiplicity ν_{post} of these postscission neutrons is a measure of the excitation energy remaining in the fragments.

Recently, Hilscher *et al.*[3,4] studied the fission dynamics of hot nuclei with composite systems $A_{CN} \geq 150$ and $E^*_{CN} \geq 50$ MeV predominantly stemming from heavy-ion induced reactions; they reached the conclusion that in fusion-fission reactions with $E^*_{CN} > 50$ MeV, the prescission neutron emission is so fast compared to the overdamped motion[2] in the scission direction that it cools this composite system down to $E^*_{CN} \approx 40-60$ MeV before the scission point is reached. As a consequence ν_{post} is expected to stay roughly constant independent of the entrance channel energy and momentum.

In this paper we want to extend the study of preneutron versus postneutron scission multiplicity to lower ($E^*_{CN} \leq 31$ MeV) excitation energies for highly ($x = 0.75$) fissile systems $p + ^{235,236,238}U$ partially already treated in the classical papers of Bishop *et al.*[5,6] on this subject at lower excitation. A study[2] of heavy-ion induced fusion-fission concluded that ν_{iso} shows a remarkably consistent and smooth trend in its dependence on E^*_{CN} and x; therefore, we intend to link our work to the result[7] that with increasing $x > 0.7$, statistical-model calculations underestimate ν_{iso} considerably for E^*_{CN} as low as 60–100 MeV. The application of proton projectiles will exclude fast fission due to a substantial reduction of the fission barrier by angular momentum effects in the entrance channel.[8]

Emphasis is put on an extension of the projectile energy range 12.7 MeV $\leq E_p \leq$ 25.5 MeV, a neutron time-of-flight spectroscopy with n-γ discrimination and on improved energy resolution, spectroscopy of the fragments with time-of-flight (TOF) techniques—giving better access[9,10] to the fragment masses m_i^* prior to neutron emission—as well as by energy in order to allow for a complete mapping of the energy flow as a function of mass split and neutron multiplicity.

With these data we are then also able to study the ν_{post} as a function of both fragment mass and excitation energy in the fragments, and thus the persistence or disappearance of the famous "sawtooth" $\nu_{post}(m)$ with the total kinetic energy (TKE). This quantity is of particular interest, because the random neck rupture model of Brosa *et al.*[11] predicts the structure to persist with growing E^*_{CN} (but shifted upward in absolute number), whereas the statistical scission point model[12] does not.

At present, there are three classes of theoretical approaches to the fission process in discussion. The statistical model of Wilkins *et al.*[12] assumes a quasistability at the scission point. It can be applied to all kinds of nuclear fission, in particular those with high mass asymmetry and those which are strongly influenced by shell effects, but it has its problems[13] with the widths of the fragment mass distributions. The liquid drop model is essentially restricted to symmetric fission[14] and therefore not very appropriate for the reaction systems under discussion. Recently, Brosa *et al.*[13] introduced a model based on a random neck rupture that naturally leads to the experimentally observed widths of mass distributions and predicts the sawtooth $\nu_{post}(m)$ as a consequence of

the asymmetric prescission shape whose origin is seen[15] as an effect of inertia and minimization of surface energy. Experimental data both in support of[16] and in conflict[17] with the resulting energy sharing as a function of mass split have been published.

Our paper is organized as follows. In Sec. II we present the experimental arrangement with emphasis on details not yet published. Section III is devoted to the experimental results and a qualitative discussion of the general trends visible in the inclusive fragment and neutron data in comparison to those of Ferguson *et al.*[18] and of Bishop *et al.*[5,6] The discussion of the results in terms of the questions already raised—in particular, (i) prescission neutron multiplicities as a function of primary excitation energy E^*_{CN} (ii) postscission neutron multiplicity as a function of fragment mass and TKE of the fragments—and in comparison to calculations performed in the statistical model of nuclear reactions is presented in Sec. IV. Section V summarizes our results and conclusions.

II. EXPERIMENTAL ARRANGEMENT

A. General setup

Two different setups have been applied. The first one, hereafter called EXSC, used scintillator foils for fragment spectroscopy by TOF. These foils are resistant against irradiation and can stand high count rates so that the three systems $p+^{235,236,238}$U could be studied at several projectile energies E_p between 12.7 and 25.5 MeV to provide a survey of neutron-fission coincidence data, however, without good fragment energy information. In the second one (EXSB) fragments were spectroscopied both in TOF (mass) *and* pulse height (energy) with large-area surface-barrier detectors; the enhanced requirements on counting statistics allowed to measure neutron-fission coincident only for $E_p=20.4$ MeV and only for $p+^{238}$U. In addition, single runs for fission fragments were performed for $p+^{235,236,238}$U and $E_p=15.2$, 20.4, and 25.7 MeV with this setup. A summary of projectile energies and targets used is given in Table I. What both setups have in common is that all neutron and fission fragment detectors and the target are positioned in a plane perpendicular to the proton beam.

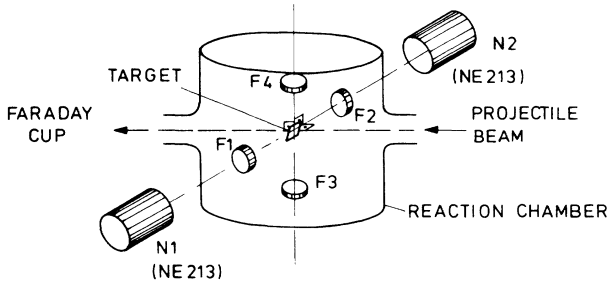

FIG. 1. Geometry of the EXSB setup.

The geometry of the EXSB arrangement is schematically shown in Fig. 1. Two fragment detectors $F1$, $F2$ define the horizontal fission axis. Neutrons are measured by means of the two independent, fixed TOF detectors $N1$ and $N2$ under the correlation angle $\Theta_c=0°$ with respect to this axis. The $\Theta_c=90°$ correlation was measured in the EXSC experiment by rotating $F1$ and $F2$ with the whole reaction chamber carrying $F1$ and $F2$ around the beam axis by 90° into the position $F3$,$F4$. In the EXSB geometry, $F3$ and $F4$ were realized by a second pair of surface-barrier detectors. For fission coincident prefission neutrons the two correlations $\Theta_c=0°$ and $\Theta_c=90°$ are equivalent, whereas the postfission neutron yield varies considerably with Θ_C. The EXSC setup and the quality of data obtained with it has been presented in two earlier papers the reader is referred to;[19,20] we mention here only that the scintillator foils representing detectors $F1$ and $F2$ were placed at TOF distances of 21.4 and 15.2 cm and subtended solid angles of 104 and 228 msr, respectively.

B. Fragment and neutron spectroscopy in EXSB geometry

The four detectors $F1$-$F4$ consisted of fully depleted material of specific resistance $\rho\approx1200$ Ωcm, were of areal

TABLE I. Summary of experiments.

Projectile energy E_p (MeV)[a]	Experimental setup	Targets[b] ^{235}U,	^{236}U,	^{238}U	Types of measurement[c] FM	NM	FME	NME
12.7	EXSC	X	X	X	X	X		
15.2	EXSB	X	X	X			X	
	EXSC	X	X	X	X	X		
18.3	EXSC		X	X	X	X		
20.3	EXSB	X	X				X	
	EXSB			X			X	X
22.3	EXSC		X	X	X	X		
25.6	EXSB	X	X	X			X	
	EXSC			X	X	X		

[a] $\Delta E_p=\pm0.1$ MeV.

[b] $^{238}UF_4$, thickness 100–150 μg/cm², on 40 μg/cm² carbon; $^{235,236}U_3O_8$, thickness 110–150 μg/cm², on 40–60 μg/cm² carbon.

[c] FM: Fragment-fragment coincidences (mass determination); NM: Neutron-fragment coincidences (mass determination); FME and NME: As before, but including fragment energy measurement, too.

size 7.0 cm^2, thickness 170 μm, and capacitance 400 pF. For operation, the detectors were cooled to -20 °C; they then showed a time resolution for fission fragments from ^{252}Cf as well as pulses from an IR laser (intrinsic width: 67 ps) of 250 ps full width at half maximum (FWHM) with the aperture being fully open.[21] The TOF path lengths to $F1$ and $F3$ were 20.3 and 17.6 cm; apertures in front of them defined the effective solid angles of 10.1 and 14.3 msr, respectively. The associated detectors $F2$,$F4$ (TOF paths: 20.3 and 17.6 cm; solid angles 17.2 and 22.8 msr) were out of the 180° correlation by $\Delta\Theta_{lab}=1.3°$ to account for the linear momentum transferred from the projectile to the composite system ^{236,237,238}Np. The broadening of the angular correlation by neutron emission from the fully accelerated fragments was accounted for by the solid angles of $F2$ and $F4$, respectively.

The targets were inclined by 45° with respect to the fission axis $\overline{F_1F_2}$ as well as $\overline{F_3F_4}$. They were held on +20 kV potential to prevent secondary electrons from reaching the detectors. The whole setup was housed in a thin-walled aluminum reaction chamber with neutron windows of 1.5 mm thickness.

Neutrons were detected with two NE213 scintillator cells of 25.4 cm $\phi\times5.1$ cm (in EXSC geometry: 10.2 cm $\phi\times5.1$ cm) coupled to XP2041 photomultipliers. The detectors were operated with n-γ discrimination,[19] with pulse-height thresholds of typically $E_n^{th}=0.65$ MeV and time resolutions of 2.1 ns (1.2 ns). The neutron TOF spectroscopy with flight paths of 1.8 m results in an overall energy resolution ΔE_n (FWHM) of 45 keV (55 keV) and 0.83 MeV (1.18 MeV) for $E_n\approx1$ and 10 MeV, respectively. The neutron detectors were heavily shielded with lead and paraffin against background and time uncorrelated radiation. Shadow bars of 0.7 m length made of polyethylene that obscured the solid angles of the detectors and provided an attenuation >99% for $E_n\leq20$ MeV were used in background runs with the target being in position. The two neutron detectors were run independently to double statistics and to get an uncertainty estimate. The neutron TOF was measured with respect to the cyclotron RF.[22]

III. MEASUREMENTS AND RESULTS

For each target and projectile energy, runs were performed for the correlation angles $\Theta_c=0°$ and 90° simultaneously (EXSB) or sequentially (EXSC). Each run was supplemented by a neutron background run. Beam intensity was typically 30–50 nA, with burst widths Δt_p varying between 0.7 ns ($E_p=25$ MeV) and 1.4 ns ($E_p=12.7$ MeV). Measurements were extended until $\approx10^5$ (6×10^4) true events were recorded for a $\Theta_c=0°$ ($\Theta_c=90°$) correlation, requiring about 10^7 fission-fission coincidences. In regular intervals, pulse-height calibrations of $F1$-$F4$ were performed with two ^{252}Cf sources replacing the target.

For each neutron-fission event, the neutron TOF $T(N)$ is stored together with the pulse heights from the pair of active fission fragment detectors F_i and F_j, and the TOF informations $T(F_i)$ and $T(F_i-F_j)$. The RF phase was monitored continuously such that phase shifts could be corrected for off line. Dead time and time calibration were monitored with the IR laser pulser that was optically coupled to all four surface-barrier detectors. Off-line data analysis was performed event wise on a PDP 11/40. Spectra representative for the coincident neutron or fission detection are shown in Fig. 2.

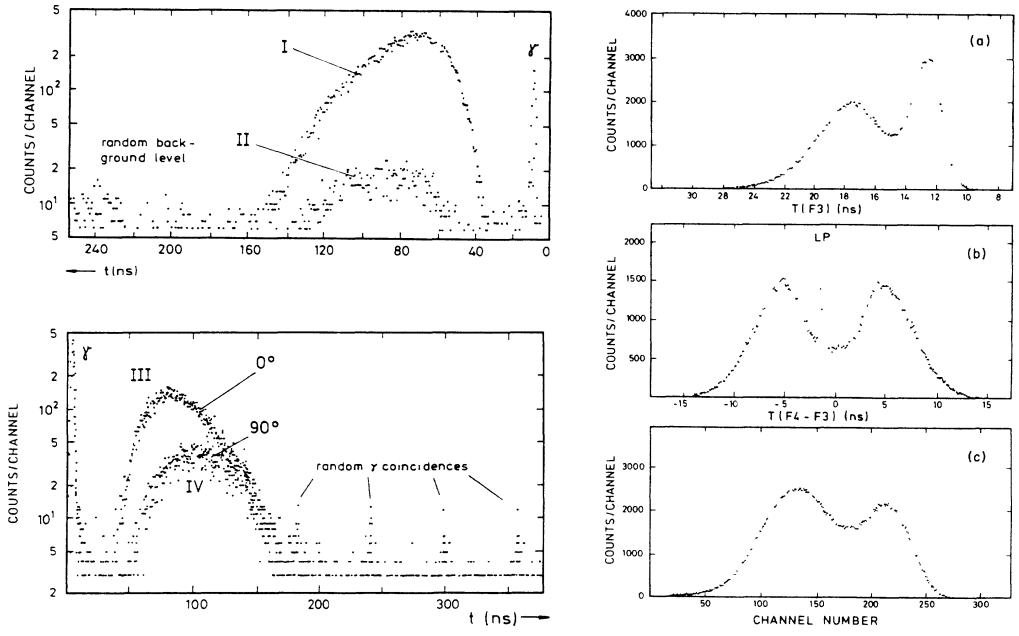

FIG. 2. Raw data of $p+^{238}$U neutron-fission coincidences at $E_p=20.3$ MeV. Left: Neutron TOF spectra; effect (I) and background (II) run, correlation $\Theta_c=0°$ (III) and 90° (IV). Data is normalized to the same fission rate. Right: Fission events observed with SB detectors: TOF spectrum (a), TOF difference spectrum (b), and pulse-height spectrum (c). LP indicates the light pulser peak.

A. Fragment mass and energy determination

Fragment masses m_i^* prior to neutron emission follow from[9]

$$m_1^* = M(1+v_1^*/v_2^*)^{-1}$$

and

$$m_2^* = M - m_1^* \ .$$

Here, M denotes the mass of the fissioning system, i.e., the compound nucleus mass with a small correction for emission of scission and prefission neutron emission that has been neglected here;[9] the velocities v_i^*, due to the isotropic emission of unobserved neutrons in the restframe of fragment i, can be approximated by the laboratory velocities v_i accessible via the flight times $T(F_i)$. The accuracy of mass determination with scintillator foils (EXSC geometry) has been discussed in Ref. 19. The TOF spectroscopy with solid-state detectors (EXSB geometry) has to cope with two corrections, namely the velocity loss of the fragments in the target material, which has been treated as a function of fragment mass and final velocity on the basis of known[23] energy-loss data, and the plasma delays. They have been taken care of with the general task to establish an absolute TOF time scale. For this purpose the symmetry point (minimum) in the $T(F_i - F_j)$ spectrum (cf. Fig. 2) is associated with symmetric fission. The pulse heights of the individual events of symmetric fission provide the knowledge of their velocities such that the time-zero point can be deduced for $T(F_i)$ as well as for $T(F_j)$, i.e., on all TOF paths.[24] For nonsymmetric fragmentations the plasma delay difference has been measured previously with our detectors.[21]

The resulting fragment mass resolution depends on the burst width Δt_p and is $\sigma(m) \simeq 1.5$–2.5 u for the EXSC geometry,[19] whereas with the surface-barrier detectors the value $\sigma(m) \simeq 1$ u was achieved in the mass range $80 \leq A \leq 160$ and $\Delta t_p \leq 0.9$ ns.

Fragment energies were determined following the prescription of Schmitt[25] with the calibration constants obtained in the ^{252}Cf runs and the coefficients replaced by those from Ref. 26; these coefficients yield total kinetic energies that are typically $\Delta E_{\rm tot} = 2.5$ MeV lower and that show consistency with the TOF measurement.[21]

B. Fission fragment properties

Ferguson *et al.*[18] have studied the fission fragment pairs from $p + ^{233,235,238}$U for protons with energies E_p between 7 and 13 MeV or initial excitations $E_{\rm CN}^*$ from 11 to 19 MeV. The main trends observed in those[18] data as a function of E_p or $E_{\rm CN}^*$, the TKE or the fragment mass m_i shall be compared to our findings for $E_p = 12.7$–25.6 MeV:

(i) The mass distributions show yields for symmetric scission increasing with E_p. The peak yields decrease and their locations shift slightly to lower heavy-fragment masses. This trend continues for $E_p = 12$–25 MeV [cf. Fig. 9 in Ref. 19]; it is more pronounced if the mass distributions are considered as a function of the TKE, i.e., for different excitation energies of the composite system at the scission point (Fig. 3).

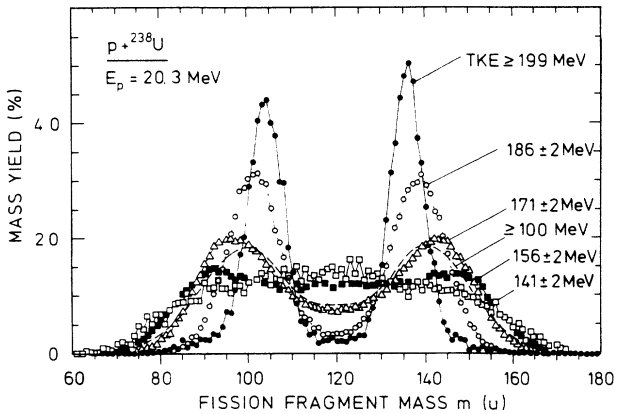

FIG. 3. Normalized fragment mass yields for the TKE windows indicated.

This observation reflects a competition of two channels leading to fission, with relative contributions that vary with $E_{\rm CN}^*$. With increasing E_p, the channel that deals with the higher barrier[12] or energy for neck rupture[28] gains relative weight. This is for ^{239}Np the super long channel[27] leading to symmetric fission. It competes favorably with the standard channel[28] for asymmetric fragmentation and with a TKE that is higher than that for the super long channel; gating on the TKE isolates the two channels more effectively than variation of $E_{\rm CN}^*$.

(ii) The average TKE as a function of mass split decreases with increasing $E_{\rm CN}^*$ in the region of the heavy fragment ($m_H^* \approx 132$ u), whereas for symmetric fragmentation this trend is reversed and persists for energies E_p up to 25 MeV (Fig. 4).

As the TKE reflects the repulsion energy of the nascent fragments from the scission point on, its decrease in the mass range $m_H^* \approx 132$ u with increasing E_p indicates[12]

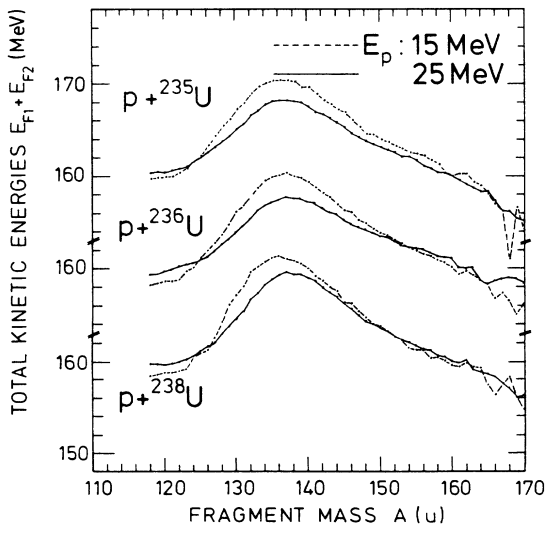

FIG. 4. Average total fragment kinetic energies as a function of the heavy fragment mass for ^{235,236,238}U(p,f) and $E_p = 15$ and 25 MeV.

TABLE II. Average total kinetic energies TKE of fragments prior to neutron emission. Also given is the value calculated from the systematic of Ref. 29.

Target	E_p (MeV)	TKE (MeV)	TKE (MeV) (Ref. 29)	Ref.
^{233}U	9.5	169.8±3	174.2	5
	14	169.3±3		5
	20	166.8±3		5
^{235}U	15.2	171.7±2	173.7	This work
	20.3	170.4±2		This work
	25.6	170.3±2		This work
^{236}U	15.2	171.0±2	173.4	This work
	25.6	169.6±2		This work
^{238}U	11.5	178.3±3	173.0	5
	18	177.2±3		5
	22	176.7±3		5
	15.2	172.2±2		This work
	20.3	170.9±2		This work
	25.6	171.0±2		This work

the relaxation of the reaction system with E^*_{CN} towards higher deformation. As a consequence, these fragments are expected to show higher intrinsic excitation stemming from the deformation converted into heat after snapping back. This argument is compatible with the random neck rupture model as well. In contrast, for symmetric mass splits the system relaxes with increasing E^*_{CN} towards smaller deformations[12] because they are favored by the Strutinsky shell correction. The broad mass distributions are, however, at variance with this explanation.[28]

(iii) The values for TKE corrected for fragment mass reduction by neutron emission[9] are given in Table II; they continue to decrease with increasing E_p for all isotopes. The absolute values of TKE show no significant dependence on the target mass.

The negative slopes of $\Delta\mathrm{TKE}/\Delta E_p$ were also observed in Ref. 5 for $p+^{233,238}$U (cf. Table II); they result from the increase (decrease) of the yield for symmetric (asymmetric) fission in combination with the trend of TKE(m) visible in Fig. 4. The absolute TKE values of Ref. 5 for $p+^{238}$U are at variance with our data; the discrepancy would be approximately 2.5 MeV smaller[21] if the pulse-height conversion coefficients of Ref. 26 instead of those from Ref. 25 could have been applied.

(iv) The root-mean-square widths $\sigma_E(m_H/m_L)$ of the TKE distributions as a function of fragmentation showed for 7 MeV $\leq E_p \leq 13$ MeV a slight increase with E_p and a maximum at $m_H \approx 126-129$ u with absolute values of 13–14 MeV and no significant target mass dependence. Our data confirms these findings quantitatively for $E_p \leq 25$ MeV (Fig. 5).

The observed width $\sigma_E(m_i)$ for a given fragmentation m_H/m_L results from the superposition of widths for the two competing fragmentation channels. In the mass region $m_H \approx 130$ u, the standard channel dominates. Here, the variance σ^2 is largest, because (a) the absolute TKE values are highest and (b) the average distances of the nascent fragments scatter most due to the competing deformed shell corrections.[12] The quantitative calculation in the framework of the random rupture model[30] leads to values slightly lower than those in Fig. 5.

Altogether it can be stated that the trends observed in Ref. 18 continue with increasing E_p although the fraction of second or higher chance fission certainly[20,31] increases. This agreement also represents an additional confirmation of absolute values for fragment energies and masses obtained in this work and applied in the further analysis.

C. Separation of prescission and postscission neutrons

In principle, each spectrum contains contributions emitted (i) from the composite system (CN), (ii) during the transition of the CN through the saddle-point

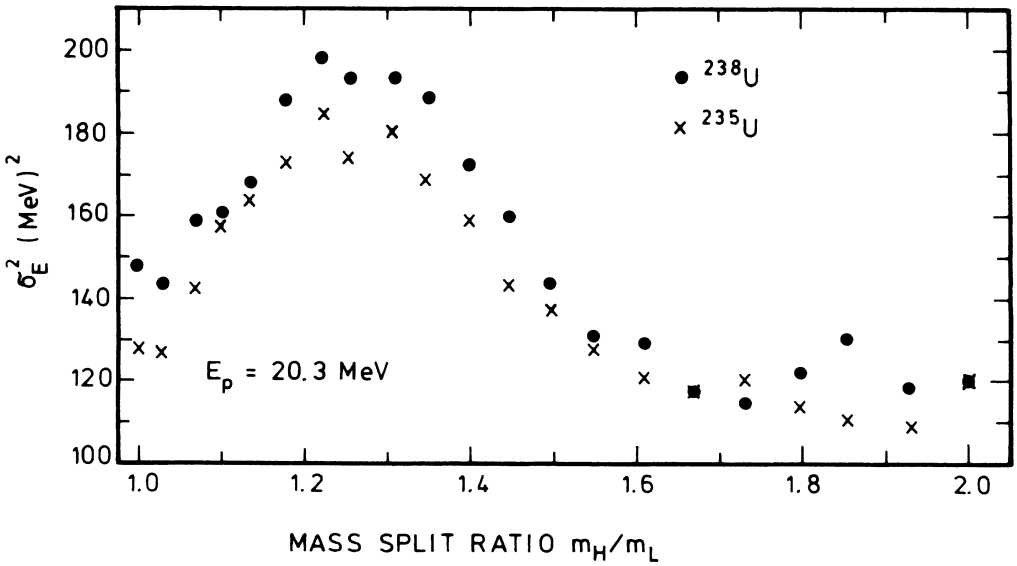

FIG. 5. Variance σ^2_E of TKE as a function of the mass split ratio m_H/m_L for ^{235,238}U(p,f) and $E_p = 20.3$ MeV.

configuration towards the scission point, (iii) during the neck rupture, (iv) from the accelerating fragments and (v) after completion of their acceleration. The contributions (i)–(iii) are experimentally not distinguishable and are therefore subsummarized as prescission neutrons; the contribution (ii) is expected to be contributed during a time of about 20×10^{-21} s for the saddle-to-scission transition.[7] The scission neutron multiplicity (iii) can be estimated from the isotropic fission neutron yield of ^{252}Cf (Ref. 6) and $p+^{226}$Ra (Ref. 32) to be $\nu_{sc}\approx0.3$. The contributions from (iv) and (v) are classified as postscission neutrons, where the contribution (iv) is expected[32,33] to be small.

The decomposition into prescission and postscission neutron energy spectra in the center-of-mass (c.m.) frame of the CN or the fully accelerated fragment, respectively, was performed under the assumption of isotropic emission in the source system. The iterative procedure is similar to that of Fraenkel *et al.*[34]

For given bins of neutron velocity v_n, fragment mass m_j and velocity v_j ($j=1,2$), the quantity A_0 may denote the experimental neutron yield obtained under $\Theta_c=0°$ with reference to fragment 1; similarly A_{90} gives the laboratory yield for $\Theta_c=90°$. Contributions to these yields come from the isotropic component x and the postscission yields $y_j(\Theta)$ of fragment j under the angle Θ:

$$A_0=y_1(0)+y_2(\pi)+x\ , \tag{1}$$

$$A_{90}=x+y_1(\pi/2)+y_2(\pi/2)\ . \tag{2}$$

As a first approximation we take

$$y_1(0)=A_0\ , \tag{3}$$

$$x=A_{90}\ , \tag{4}$$

with Eq. (3) leading to y via

$$y=T(0\rightarrow\text{c.m.})y_1(0)\ . \tag{5}$$

Here, the transformations $T(\Theta\rightarrow\text{c.m.})$, and similarly

$$T^2(\Theta_1\rightarrow\Theta_2)=T(\text{c.m.}\rightarrow\Theta_2)\times T(\Theta_1\rightarrow\text{c.m.})\ ,$$

make use of the known source velocities. The isotropic yields x,y in the respective center-of-mass systems are obtained by iterating Eqs. (3)–(5). For the first iteration, Eqs. (3) and (4) are inserted into Eqs. (1) and (2), yielding

$$x=A_{90}-2\times T^2(0\rightarrow\pi/2)A_0 \tag{6}$$

$$y_1(0)=A_0-T^2(0\rightarrow\pi)A_0-[A_{90}-2\times T^2(0\rightarrow\pi/2)A_0] \tag{7}$$

and subsequent construction of y with Eq. (5). We found that further iterations do not improve the results. For y, Eq. (3) is already a good approximation and the correction introduced by Eq. (7) is small. For x, the approximation in Eq. (4) is a factor of about 3 too small, because the three terms in Eq. (2) are of comparable size; therefore Eq. (6) represents the essential correction. Here application of improved values for y_1,y_2 modify the results only within the statistical uncertainties. The procedure was actually applied eventwise.

A representative result for one neutron detector is shown in Fig. 6. The dashed line in the upper part separates the contribution of the fragment flying in the opposite ($\Theta_c=180°$) direction. For further analysis, the spectra of both neutron detectors for a given reaction system were combined to give the total multiplicities $\nu_{post}(E_n)$ and $\nu_{iso}(E_n)$ per fission *event* and neutron energy bin, and postscission multiplicities $\nu_{post}(m)$ per fission *fragment* of mass m.

In Fig. 7 we present the resulting multiplicities. A first glance shows Maxwellian spectral shapes with no significant differences between the three uranium isotopes. It is, however, interesting to note that with increasing primary excitation energy E^*_{CN} postscission *and* prescission multiplicities increase with comparable rates. In order to perform this comparison more quantitatively, the data $\nu_{iso}(E_n)$ must be supplemented for the fraction the experiment missed due to the neutron threshold $E_n^{th}\approx0.65$ MeV, cf. Fig. 6. We will show that this correction is in the order of 20%. For the postscission

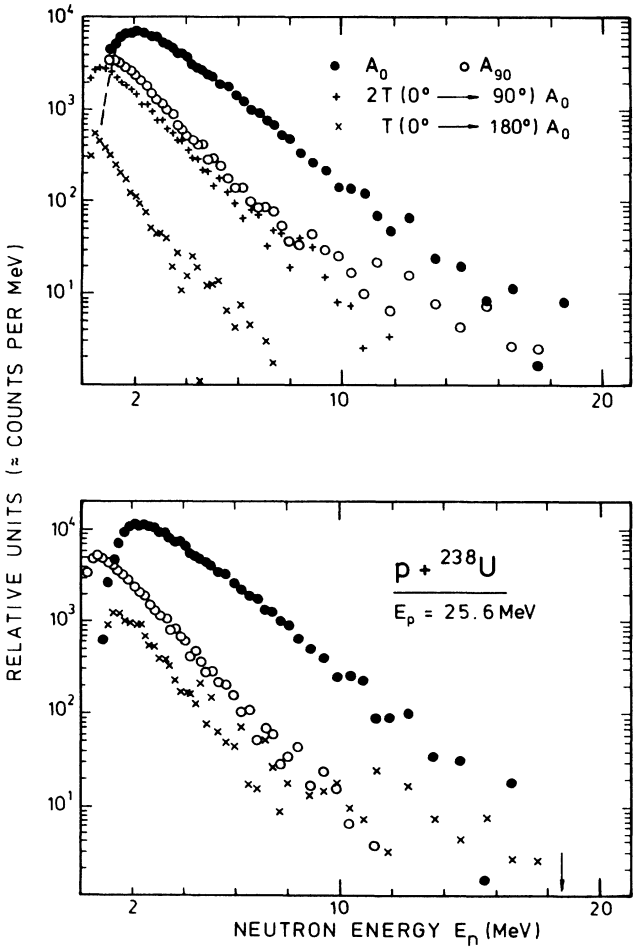

FIG. 6. Decomposition of neutron energy spectra for $p+^{238}$U at $E_p=25.6$ MeV. Upper part; Experimental laboratory results A_0 and A_{90} and intermediate results entering into Eqs. (6) and (7). Lower part; Resulting postscission component in the lab system for $\Theta_c=0°$ (●) and the fragment cms system (○), and the prescission component (x). The arrow indicates the high-energy limit of prescission neutrons for $B_f=6.2$ MeV.

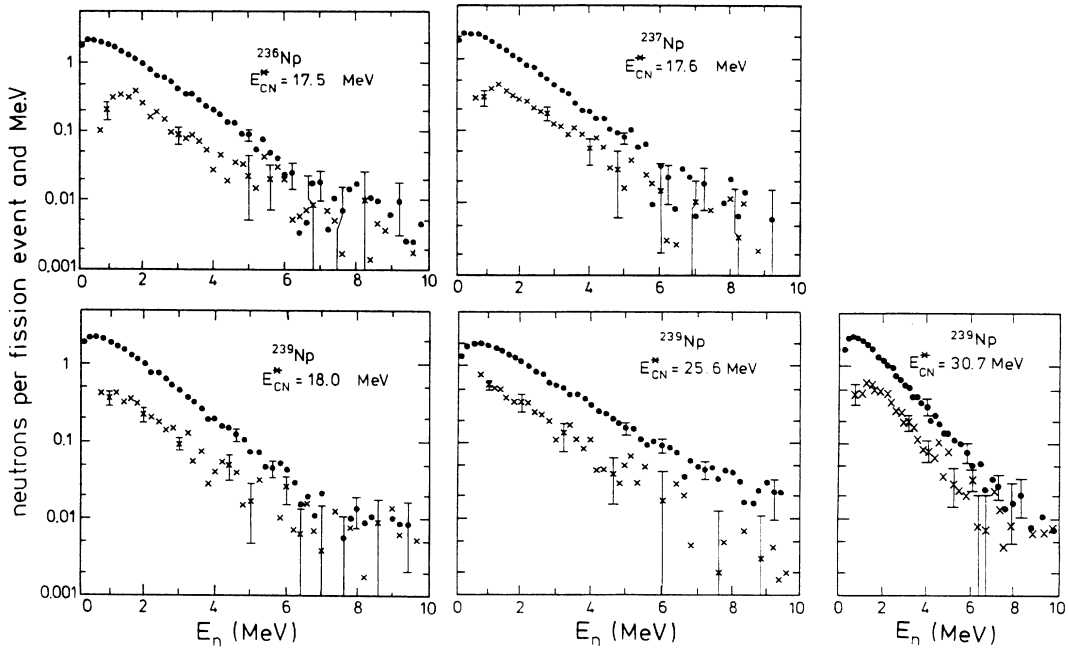

FIG. 7. Neutron multiplicities $\nu_{iso}(E_n)$ (×) and $\nu_{post}(E_n)$ (●) for all reaction systems studied in EXSB and one (^{239}Np at $E^*_{CN}=30.7$ MeV) in EXSC geometry. The EXSC results not shown are of similar quality.

component, no such correction is required. It is, however, necessary to condense the information of Fig. 7 into a few parameters. This will be done in the next section. Before, a few comments on the systematic errors in the separation into prescission and postscission multiplicities are in order.

The postscission component is assumed to stem from isotropically emitting, fully accelerated fragments. Neutrons emitted during the acceleration of the fragments tend to lower the resulting values ν_{post}; the effect is, however, negligibly ($\leq 2\%$) small.[33] In order to estimate the maximum impact of nonisotropic neutron emission we introduced a distribution[35,36]

$$\omega(\Theta_c)=1+\epsilon\cdot\cos^2\Theta_c$$

with $\epsilon \leq 0.1$ in the separation procedure. It results in a reduction of ν_{post} by $\leq 7\%$, but does not influence $\bar{E}_{n,post}$ nor the fragment mass dependence $\nu_{post}(m)$. However, as a consequence of neutron multiplicity conservation, the values for ν_{iso} increase by 0.10–0.17 neutrons per fission, i.e., 10–20 %. This increase is in first order the same for all projectile energies E_p and is therefore equivalent of a global increase of ν_{sc}; it does not influence the dependence of ν_{iso} on E_p or E^*_{CN}.

1. *Parametrization of prescission and postscission neutron spectra*

The results in Fig. 7 indicate prescission multiplicities of no more than about one neutron/fission. Therefore,

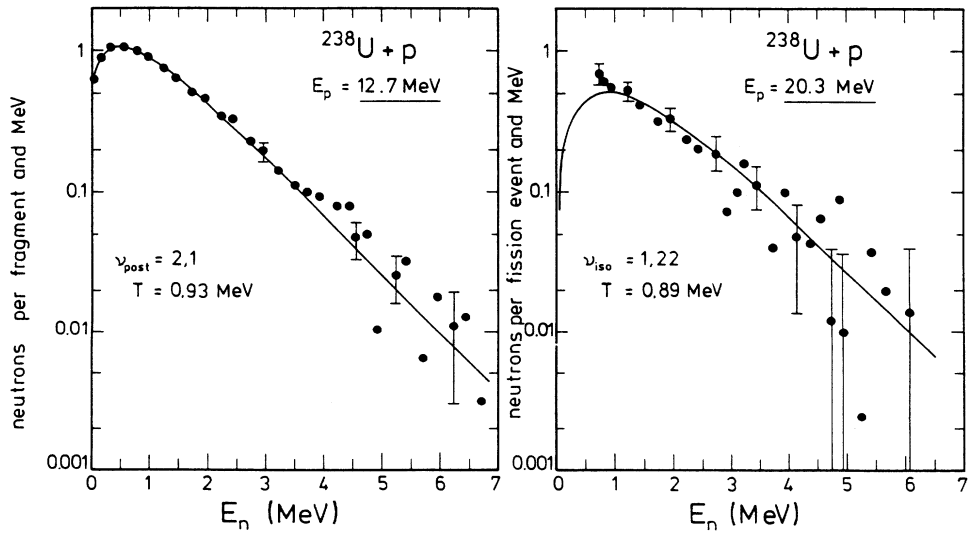

FIG. 8. Fits to a prescission and postscission spectrum of neutron detector $N1$.

TABLE III. Average values of neutron multiplicities ν_{post} and ν_{iso} per fission event, neutron energies $\bar{E}_{n,post}$ and $\bar{E}_{n,iso}$, and nuclear temperatures T and T_{CN} obtained directly from the experimental data and from a neutron source fit, respectively.

		Postscission neutrons					Isotropic component				
Compound	E^*_{CN}	Experiment		Fit, Eq. (9)			Experiment		Fit, Eq. (8)		
nucleus	[MeV]	ν_{post}	$\bar{E}_{n,post}$	ν_{post}	$\bar{E}_{n,post}$	T	ν_{iso}	$\bar{E}_{n,iso}$	ν_{iso}	$\bar{E}_{n,iso}$	T_{CN}
^{239}Np	17.9	4.26	1.48	4.22	1.40	0.93	0.63	2.31	0.75	1.82	0.91
	18.04	4.32	1.51	4.30	1.44	0.96	0.71	2.17	0.87	1.79	0.89
	20.5	4.54	1.47	4.54	1.42	0.94	0.84	1.92	0.92	1.51	0.75
	23.5	4.84	1.60	4.70	1.50	1.00	0.90	2.28	1.29	1.66	0.83
	25.6	4.82	1.88	4.79	1.73	1.15	1.04	2.27	1.38	1.77	0.89
	27.5	4.89	1.61	4.86	1.53	1.02	1.22	2.22	1.37	1.62	0.87
	30.7	5.20	1.66	5.14	1.54	1.02	1.23	2.59	1.48	1.83	0.91
^{237}Np	17.5	4.11	1.48	4.10	1.39	0.93	0.55	2.38	0.64	1.95	0.98
	17.64	4.31	1.49	4.28	1.41	0.94	0.77	2.18	0.93	1.81	0.90
	20.1	4.30	1.54	4.28	1.45	0.97	0.82	2.00	0.96	1.60	0.80
	23.1	4.53	1.59	4.50	1.50	1.00	0.92	2.22	1.12	1.60	0.80
	27.1	4.85	1.61	4.82	1.52	1.02	1.21	2.23	1.33	1.64	0.82
^{236}Np	17.4	4.12	1.51	4.08	1.42	0.94	0.59	1.98	0.71	1.92	0.96
	17.54	4.21	1.54	4.30	1.46	0.97	0.63	2.04	0.80	1.71	0.83
	20.0	4.30	1.54	4.30	1.46	0.97	1.00	2.08	1.04	1.71	0.85
Uncertainty		±0.15	±0.04	±0.10	±0.03	±0.02	±0.15	±0.18	±0.16	±0.12	±0.06

the evaporation spectrum can be described in the CN frame of reference as[37]

$$\frac{dN}{dE_n} = \frac{\nu_{iso}}{T_{CN}^2} E_n \exp\left[-\frac{E_n}{T_{CN}}\right] \tag{8}$$

with the parameters ν_{iso} and T_{CN}. The average neutron energy $E_{n,iso}$ is then 2 T_{CN}.

For the postscission component we have $\nu_{post} > 1$ and therefore sequential neutron emission, which is approximated in the fragment system by[37]

$$\frac{dN}{dE_n} = \frac{2}{\sqrt{\pi}} \frac{\nu_{post}}{T^{3/2}} \sqrt{E_n} \exp\left[-\frac{E_n}{T}\right], \tag{9}$$

which leads to $\bar{E}_{n,post} = 1.5$ T. The temperature parameter T is a factor $\frac{12}{11}$ smaller than the initial fragment temperature T_0. We have applied Eqs. (8) and (9) to fit the data presented in Fig. 7 in the energy range $E_n \leq 7$ MeV, and two representative results are shown in Fig. 8. A summary of all fit parameters is given in Table III. For the postscission component, the experimental and the fit results for ν_{post} and $\bar{E}_{n,post}$ agree satisfactorily. The systematic differences between both sets of results for the isotropic component are due to neutrons with laboratory energies $E_n < E_n^{th}$ missing in the experimental data; after correction, the multiplicities are consistent within 5%.

2. *Dependence on* E^*_{CN}

The data in Table III show that the multiplicities ν_{post} as well as the fragment temperatures T increase for all three reaction systems with the initial excitation energy E^*_{CN}. The result $\Delta E^*_{CN}/\Delta\nu_{post} = 15.2 \pm 1.5$ MeV/n of a least squares fit (Fig. 9) is about a factor of 2 higher than

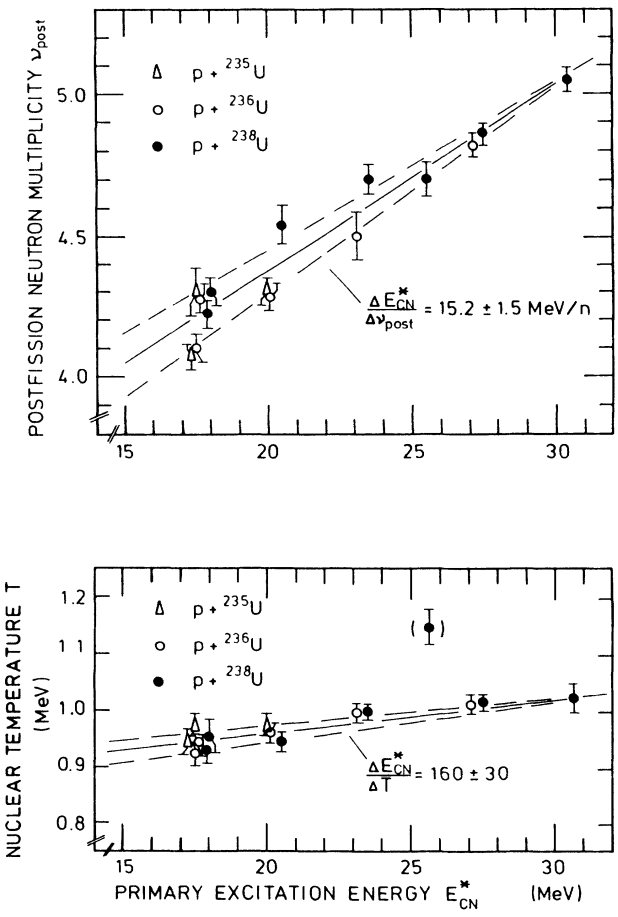

FIG. 9. Postscission neutron multiplicities ν_{post} and fragment nuclear temperatures as a function of the primary excitation energy E^*_{CN} of the reaction systems $p + ^{235,236,238}$U.

one would estimate from the average neutron kinetic ($\bar{E}_{n,\mathrm{post}}$) and separation ($S_n$) energy. The lower panel in Fig. 9 shows that indeed less than 50% of the additional initial excitation energy ΔE^*_{CN} is transferred to the fragments; the fragment nuclear temperature T rises considerably slower than anticipated for an equilibrated Fermi gas with $E^*_{\mathrm{frag}}=aT^2$: Putting $E^*_{\mathrm{frag}}=E^*_{\mathrm{CN}}\times A_{\mathrm{frag}}/A_{\mathrm{CN}}$ and $a=A/8\ \mathrm{MeV}^{-1}$ yields

$$\frac{dE^*_{\mathrm{CN}}}{dT}=\frac{A_{\mathrm{CN}}}{A_{\mathrm{frag}}}2\,a_{\mathrm{frag}}\,T=2\,a_{\mathrm{CN}}\,T\approx 60\ . \qquad (10a)$$

As the TKE is nearly independent from E_p, a substantial deexcitation must already occur prior to scission. Figure 10 does indeed show, that ν_{iso} increases with E^*_{CN} at a rate comparable to that for ν_{post}. In order to correct the estimate Eq. 10(a) for prescission neutron emission, E^*_{CN} has to be replaced by

$$E^*_{\mathrm{CN}}[1-\nu_{\mathrm{iso}}(E^*_{\mathrm{CN}})(\bar{E}_{n,\mathrm{iso}}+\bar{S}_n)/E^*_{\mathrm{CN}}]\ .$$

From Fig. 10 we read for $p+^{238}\mathrm{U}$: $\Delta\nu_{\mathrm{iso}}=\Delta E^*_{\mathrm{CN}}/19$ MeV/n and obtain with $\bar{S}_n(^{239}\mathrm{Pu})=6.2$ MeV and $\bar{E}_{n,\mathrm{iso}}=1.7$ MeV (Table III) a reduction of E^*_{CN} at the scission point by a factor 0.6. The effective slope in Fig. 9(b) is therefore

$$\frac{\Delta E^*_{\mathrm{CN}}}{\Delta T}=(160\pm 30)\times 0.6=96\pm 18\ . \qquad (10b)$$

This value still exceeds the estimate [Eq. 10(a)] beyond the uncertainty stated.

We conclude from these qualitative results that already for excitation energies E^*_{CN} in $^{236,238,239}\mathrm{Np}$ as low as 17–30 MeV neutron emission competes favorably with fission on a nuclear time scale.[1,3]

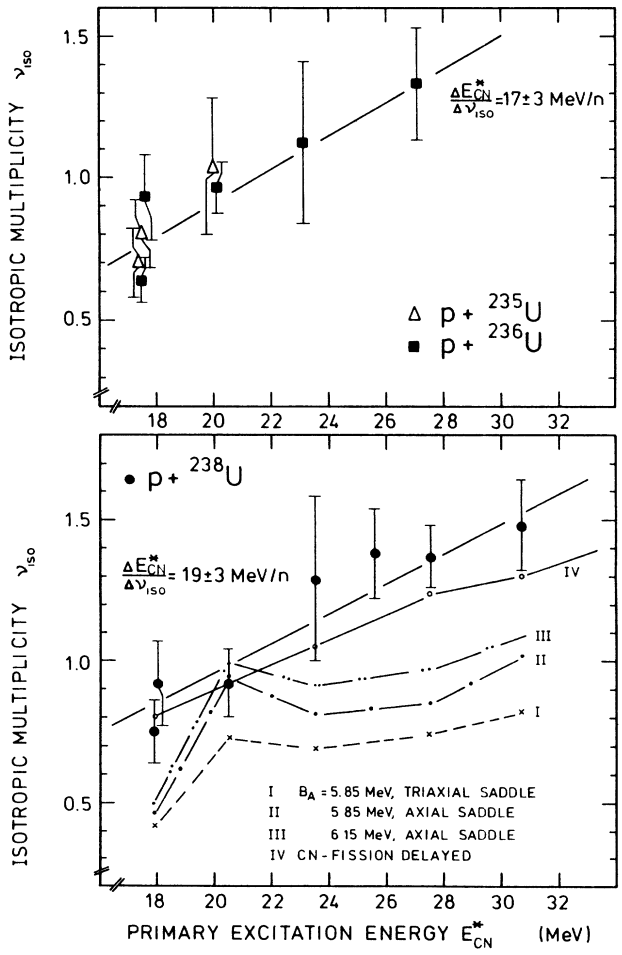

FIG. 10. Isotropic neutron multiplicity ν_{iso} for $p+^{235,236,238}\mathrm{U}$ as a function of E^*_{CN}. The straight lines denote the linear fits with the indicated slopes. The curves labeled I–III and IV denote statistical model calculations without and with a phenomenological delay for the fission competition, respectively. See Sec. IV A for details.

IV. DISCUSSION

So far, emphasis was put on the experimental results of *either* fragment *or* fission neutron measurement. In Sec. IV A we shall put these two pieces of information together to discuss ν_{post} as a function of both, fragmentation and TKE. For this purpose it is important to check beforehand that the TKE of the fragments and their excitation energies—as measured via postscission neutron emission—are mutually consistent.

The sum of the total energy released in fission as TKE and fragment excitation energies $E^*_1(m_1)$, $E^*_2(m_2)$ can be written as

$$\mathrm{TKE}(m_1,m_2)+E^*_1(m_1)+E^*_2(m_2)=Q_{\mathrm{eff}}+S_p\ , \qquad (11)$$

where S_p is the separation energy of the projectile proton from the compound system of mass m_{CN}, and

$$Q_{\mathrm{eff}}=Q(m_{\mathrm{CN}},m_1,m_2)+E_p-\nu_{\mathrm{iso}}(S_n+\bar{E}_{n,\mathrm{iso}})\ . \qquad (12)$$

As an example we shall consider the system $p+^{238}\mathrm{U}$ at $E_p=20.5$ MeV (where $\nu_{\mathrm{iso}}=0.92$ and $\bar{E}_{n,\mathrm{iso}}=1.51$ MeV, cf. Table III) for two fragmentations, namely (i) symmetric scission and (ii) the more probable fragmentation $m_1=104$ u, $m_2=134$ u.

The data to these fragmentations have been grouped into $\Delta\mathrm{TKE}=5$ MeV bins, and for each of these classes of events the total excitation energy has been derived from the postscission neutron multiplicities $\nu_{\mathrm{post}}(m_i,\mathrm{TKE})$ as

$$E^*=E^*(m_1)+E^*(m_2)=\sum_{i=1}^{2}[\nu_{\mathrm{post}}(m_i,\mathrm{TKE})(\bar{S}_n+\bar{E}_{n,\mathrm{post}})+E_{\gamma i}]\ . \qquad (13)$$

The γ emission contributes with E_γ to the deexcitation; as the γ channel has not been observed in our experiment, we took the approaches $E_\gamma=0.7\cdot\bar{S}_n$ (Ref. 38) and $E_\gamma=1.1\times\nu_{\mathrm{post}}(m,\mathrm{TKE})+1.75$ MeV (Ref. 39), respectively.

Figure 11 shows the excitation energy E^* of Eq. (13) as a function of the TKE prior to[9,40] neutron emission. For $\mathrm{TKE}>155$ MeV the experimental results scatter within $\Delta E\le 5$ MeV around the solid line representing the right-hand side of Eq. (11) with $Q(m_{\mathrm{CN}},m_1,m_2)$ being calculated from[41] for both fragmentations under consideration (the values happen to be the same). Systematic deviations occur only for $\mathrm{TKE}<155$ MeV, in particular for the

asymmetric fragmentation. The surplus of excitation energy may—according to Eq. (13)—be due to too high postscission multiplicities. If the $\nu_{post}(m_i, \mathrm{TKE})$ were systematically too high by 7% as a consequence of nonisotropic emission (cf. Sec. III C and Ref. 35), the resulting E^* would be lowered by 6 MeV (3 MeV) for TKE $\simeq$ 145 MeV (175 MeV) that would improve the agreement. Altogether, however, Fig. 11 demonstrates that neutron, γ, and fragment emission essentially exhaust the available energy.

A. Prescission multiplicity and the fusion-fission timescale

As shown in Fig. 10, ν_{iso} rises linearly for $E^*_{CN} \leq 30$ MeV with

$$\Delta E^*_{CN}/\Delta\nu_{iso} = 19\pm3(17\pm3)\ \mathrm{MeV}/n$$

for $p+^{238}$U ($p+^{235,236}$U). The slope as well as the absolute values ν_{iso} are in quantitative agreement with the results for $\nu_{pre}(E^*_{CN})$ found for heavy-ion induced fusion-fission reactions forming composite systems with $Z=92-96$ and $E^*_{CN}=50-140$ MeV [Fig. 3(b) in Ref. 2]. Such a monotonic rise is known from heavy-ion induced fusion-fission for the broader range $x\approx0.60-0.85$ of fissilities;[7] it is the less compatible with the static transition state picture the higher the excitation energy and/or fissility is. Consistency within a statistical-model calculation could only be obtained by delaying the onset of fission (by 70×10^{-21} s) or slowing the saddle-to-scission transition (30×10^{-21} s), or both (each 20×10^{-21} s). Similarly, a minimum fusion-fission time scale of 30×10^{-21} s was deduced in Ref. 3.

We want to show here with a detailed statistical-model calculation, that the equilibration in all degrees of freedom—in particular those of neutron emission and fission—is even not obtained in $p+^{238}$U for excitation energies $E^*_{CN} \geq 20$ MeV. Herefore we used the code GIVAB (Refs. 42 and 43) that considers competing deexcitation by sequential neutron and γ emission and by fission. It is based on nuclear potential surfaces represented by parabolic double humped barriers as a

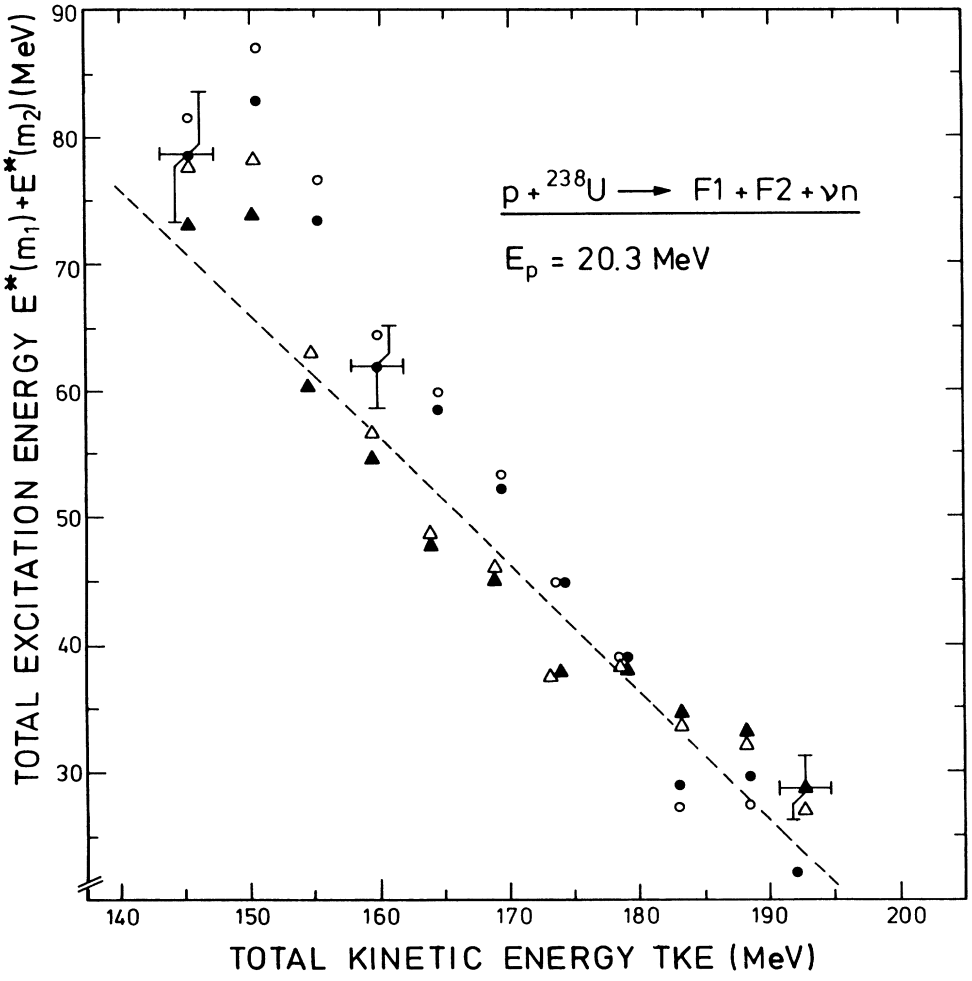

FIG. 11. Total excitation energy $E^*(m_1)+E^*(m_2)$ released in n and γ emission vs TKE prior to neutron emission. The symbols refer to symmetric (▲,△) and asymmetric (●,○) fragmentation with a contribution $E_\gamma=0.7\ S_n$ (solid symbols) and $E_\gamma=1.1\times\nu_{post}(m,\mathrm{TKE})+1.75$ MeV (open symbols), respectively. The solid line gives the result of Eq. (11) with $Q_{eff}+S_p=215.5\pm1$ MeV for both fragmentations.

function of one deformation coordinate; their parameters (three heights, three curvatures) were taken or extrapolated from fission studies with direct reactions.[44] The excited nuclei involved are assumed to have transient existence in either of the two minima. For the entrance channel, compound nucleus formation was calculated from optical-model transmission coefficients.[45] The partial widths of the decay modes from and to both wells were calculated with the following input.

(i) Transmission coefficients for neutrons were calculated with an optical-model routine and standard parameter sets; for the transmission across the parabolic barriers, the closed Hill-Wheeler expression was used. For γ emission, only electric dipole transitions were considered and, based on experimental γ widths, reduced by a factor 50 below the Weisskopf pure single-particle estimate reflecting the retardation of dipole transitions in the deformed nuclei near $A \approx 240$.[42]

(ii) The intrinsic quasiparticle state densities $\omega(E)$, spin cutoff parameters $\sigma_{\parallel}(E)$ and pairing energies were derived[43] from the theoretical single-particle level spectra for ^{244}Pu (Ref.46) at the respective nuclear deformations. The spin cutoff parameter $\sigma_{\perp}(E)$ related to the momentum of inertia perpendicular to the nuclear symmetry axis was given the value $5.45\hbar$.[43] The final level densities are obtained by application of collective enhancement factors for low-lying rotational bands on the intrinsic states.[47] As in Ref. 46 we have assumed axially symmetric shapes for the first and second well,

$$\rho_1(E,J)=\frac{\omega(E)}{\sqrt{8\pi}\sigma_{\parallel}(E)} \times \sum_{K=-J}^{+J} \exp\left[-\frac{K^2}{2\sigma_{\parallel}^2(E)}-\frac{J(J+1)-K^2}{2\sigma_{\perp}^2(E)}\right] \tag{14}$$

triaxial shapes, i.e., no symmetry at all, for the inner barrier,

$$\rho_2(E,J)=\omega(E) \times \sum_{K=-J}^{+J} \exp\left[-\frac{K^2}{2\sigma_{\perp}^2(E)}-\frac{J(J+1)-K^2}{2\sigma_{\parallel}^2(E)}\right] \tag{15}$$

and axial symmetry without mass symmetry for the outer barrier,

$$\rho_3(E,J)=2\rho_1(E,J) . \tag{16}$$

The calculations were performed for several projectile energies E_p yielding the cross sections $\sigma_i(E_p)$ for i^{th} chance fission of the composite system; the prescission neutron multiplicity is then obtained as

$$\nu_{\text{pre}}(E_p)=\sum_{i=1}^{4}(i-1)\times\frac{\sigma_i(E_p)}{\sigma_F(E_p)} , \tag{17}$$

where

$$\sigma_F(E_p)=\Sigma\sigma_i(E_p)$$

denotes the total fission cross section. For comparison with the experimental values of ν_{iso}, the multiplicity $\nu_{\text{sc}}\approx 0.3$ of the scission neutrons has to be added:

$$\nu_{\text{iso}}(E_p)=\nu_{\text{sc}}+\nu_{\text{pre}}(E_p) . \tag{18}$$

The curve labeled I in Fig. 10 represents the result. It underestimates the experimental values and predicts for $E^*_{\text{CN}} \geq 20$ MeV essentially a constant isotropic multiplicity in contrast to the slope observed. Britt *et al.* pointed out[48] that the shape at the inner saddle might undergo a transition to axial symmetry with increasing excitation, because the shell effects responsible for the asymmetry wash out. This increase in symmetry would lower the level density and therefore the fission probability. If this occurs—and there are indications in support of this speculation[49]—curve II should be considered instead. It does indeed show an enhanced isotropic component, but again fails to reproduce the dependence on E^*_{CN}. This discrepancy remains if the height B_A of the inner barrier is increased by 300 keV which is the quoted[44] uncertainty (curve III). The observed monotonic rise of ν_{iso} with E^*_{CN} is from $\sim$20–25 MeV in an obvious contrast with the predictions of a statistical model.

In passing we mention that this discrepancy cannot be due to preequilibrium (PE) decay modes, because the experiment with its neutron detectors at $\Theta_{\text{lab}}=90°$ is not sensitive to PE neutrons and the PE depletion of the cross section for compound nucleus formation cancels in Eq. (17).

For our system ^{239}Np at the highest excitation energy $E^*_{\text{CN}}=30.7$ MeV the multiplicity $\nu_{\text{post}}=5.20$ and the fragment temperature $T=1.02$ MeV correspond via Eq. (13) to an excitation energy

$$E^*(m_1)+E^*(m_2)\approx 60 \text{ MeV} .$$

This is close to the values found for symmetric scission of the much hotter systems ^{32}S+^{144,154}Sm (Ref. 4) or ^{32}S+^{197}Au (Ref. 50) for $E_{\text{lab}}(^{32}\text{S})=838$ MeV and full linear momentum transfer. From the low value of ν_{post} for the latter and other reactions in the range $Z=85$–91 and 77–78 it has been concluded, that most of the excitation energy of the highly excited system is removed by the evaporation of light particles prior to scission.[1]

Statistical-model calculations are therefore only capable of reproducing the number ν_{pre} of neutrons observed for excitation energies $E^*_{\text{CN}} \leq E^*_{\text{CN,thr}}$. Analysis of a variety of heavy-ion induced fusion-fission reactions with $Z=85$–91 yielded[1] that the minimum time required for neutron emission is $\geq 10^{-19}$ s for $E^*_{\text{CN}} \leq 50$ MeV, if a level density ratio $a_f/a_n=1.02$ is adopted. Only in this regime of low excitation the time is sufficiently large compared to times for saddle-to-scission transition or the delay at the saddle point configuration[1,2] to allow a statistical interpretation. However, in contrast to the dynamic time scales, the threshold value $E^*_{\text{CN,thr}}$ depends on the fissility. It descends[51] from $\sim$40 MeV for ^{213}Fr to $\sim$20 MeV for ^{251}Es and should therefore be for ^{239}Np close to 25–30 MeV. This is confirmed with our results for $p+^{238}$U in Fig. 10.

Accordingly, the delay in fission competition has to be taken care of at least in an approximate way. The diffusion model of Grange *et al.*[52] on fission dynamics assumes that the nuclear single-particle degrees of freedom equilibrate in times that are short in comparison with those (τ) of the fission variables. This delay is described in terms of a friction coefficient $\beta = 1/\tau$ that causes an exponential damping.

This overdamped motion on the path towards scission as a consequence of strong nuclear dissipation may be implemented into a statistical-model description by adding a phenomenological delay time for fission competition as was done in Ref. 7 with an analytical expression similar to that of Ref. 52 for the relaxation time for coupling the fission degrees of freedom to the nuclear thermostat. For the same purpose, the time necessary to open the fission channel may be delayed by an amount Δ. Westmeier *et al.*[53] derived it from a comparison of the width for single-particle emission with the energy of a nuclear β-quadrupole vibration and scaled it accordingly with excitation energy and compound nuclear mass. The absolute value has been fixed with a fit for $^{12}C + ^{182}W$.

This extension was added to the code WEGI (Refs. 53 and 54), which was here applied with the standard parameter values and 5×10^{-3} times the Weisskopf value for the γ width of dipole and quadrupole transitions, respectively. The calculations reproduce the known[31] fission cross sections $\sigma_F(E_p)$ satisfactorily. The isotropic multiplicities $\nu_{iso}(E_p)$ resulting from Eqs. (17) and (18) are shown as curve IV in Fig. 10. The improvement obtained by introducing the phenomenological delay Δ is obvious; in particular, the increase of ν_{iso} with E^*_{CN} is now reproduced within this phenomenologically modified statistical model. It indicates that a statistical model alone most probably is not capable to yield agreement for $E^*_{CN} \geq 20$ MeV, because actually Δ is a mockup of dynamical effects in the order of $3 \times 10^{-20} - 10^{-19}$ s on the nuclear timescale.

B. Postscission multiplicity dependence on fragment masses and TKE

A selection of results obtained for $\nu_{post}(m)$ is shown in Fig. 12. In the upper part we compare data for $p + ^{235,238}U$ at initial excitation energies E^*_{CN} of 17.4 and 17.9 MeV, respectively. The data exhibit the sawtooth structure well known from spontaneous and slow neutron induced fission. For ^{238}U they are in good agreement with the results of Bishop *et al.*[5] Our data for $^{235}U + p$ show great resemblance with those for ^{238}U, whereas in Ref. 5 the $p + ^{233}U$ data in contrast showed a sawtooth much less pronounced even for E_p as low as 9.5 MeV. We relate this difference to the fact that $^{236}Np^*$ and $^{239}Np^*$ undergo to a considerable fraction higher chance fission, whereas for $^{233}U + p$ the first chance fission dominates;[31] the low ν_{iso} values for $p + ^{233}U$ (Refs. 6 and 20) compared to $p + ^{235,238}U$ point in the same direction. Accordingly the fragments of $p + ^{233}U$ are equipped with more excitation energy and show a less pronounced sawtooth.

The structure is interpreted in the scission point model[12] in terms of shell effects in the nascent fragments and should therefore disappear with higher excitation energies. The random neck rupture model[11] traces the sawtooth back to the fluctuating position of minimum neck diameter where rupture starts and therefore to a variety of deformations of the nascent fragments that convert into a broad range of excitation energies of the accelerated fragments. As a consequence, the postscission neutron sawtooth is predicted to persist—although shifted upward—at excitation energies E^*_{CN} of more than 30 MeV.

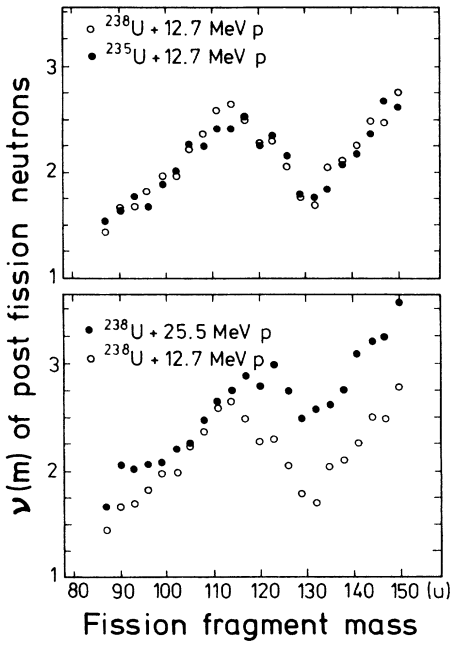

FIG. 12. Postscission neutron multiplicities versus fragment mass for different reaction systems of this work.

We therefore look into the dependence of $\nu_{post}(m)$ on fragment excitation energy. The lower panel of Fig. 12 shows that the heavier fragment benefits much more from the additional projectile energy than does the light one. A more quantitative measure is the average gradient $d\nu_{post}(m)/dE_p$ obtained from a linear regression (Fig. 13). If the fragments were in a quasistationary equilibrium at the scission point, we could expect

$$\Delta E^*(m) \sim m \Delta E^*_{CN} \ . \tag{19a}$$

The total kinetic energies being almost independent of E_p (cf. Table II) we may approximate ΔE^*_{CN} by ΔE_{proj}, and Eq. 19(a) converts into

$$\frac{\Delta E^*(m)}{\Delta E^*_{CN}} \sim \frac{\Delta \nu_{post}(m)}{\Delta E_{proj}} \sim m \ , \tag{19b}$$

whereas the data in Fig. 13 show quite a different trend.

In order to further test this behavior we have chosen a more direct way to vary the initial excitation of the fragments, namely by selecting fission events by masses m_i *and* total kinetic energy TKE. The results are shown in Fig. 14. For TKE > 182 MeV the sawtooth, though lack-

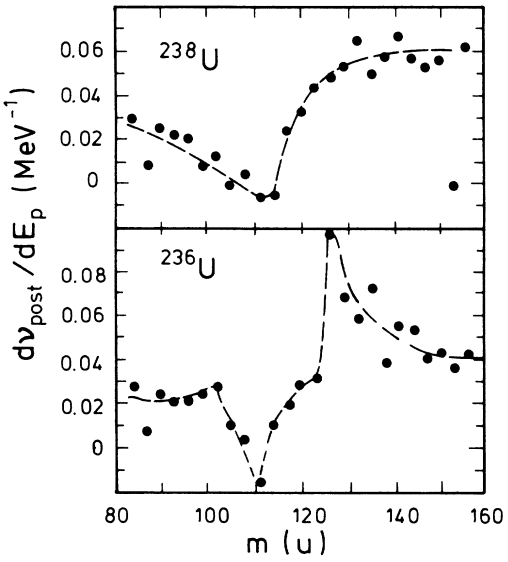

FIG. 13. Variation $d\nu_{post}(m)/dE_p$ of postscission multiplicity with projectile energy for $p+^{236,238}U$. The line is to guide the eye.

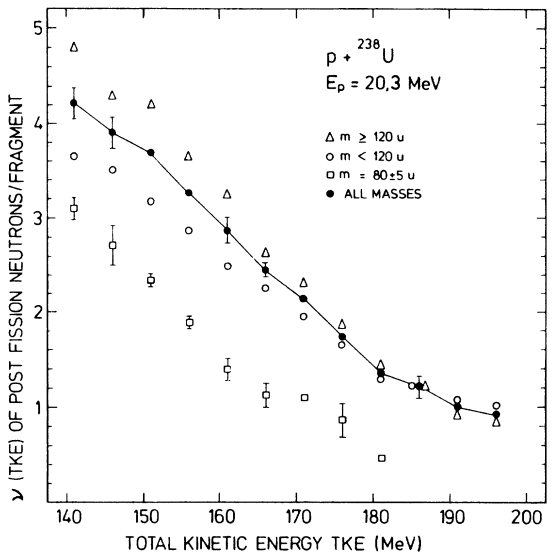

FIG. 15. Postscission neutron multiplicity per fragment as a function of TKE for different fragment mass ranges. The solid line connects the curve for all masses and has an average slope $d\text{TKE}/d\nu_{post}$ of 6.9 MeV/n for 140 MeV $\leq$ TKE $\leq$ 185 MeV.

ing in accuracy due to the reduced neutron statistics, is very pronounced, whereas $\nu_{post}(m)$ approaches the proportionality of Eq. 19(b) for TKE < 157 MeV with little sawtooth-like structure remaining. This result shows great resemblance with that[33] for $p+^{238}U$ at $E_p=155$ MeV; it would not change qualitatively, if the cut for a constant TKE were replaced by TKE values varying as point-charge Coulomb energies[55] with fragmentation, adjusted to the measured value for a symmetric mass split, because this smooth correction $\Delta\text{TKE}(A)$ amounts to less than 4 MeV for $90 \leq A \leq 145$. Also, a slight[2,56]

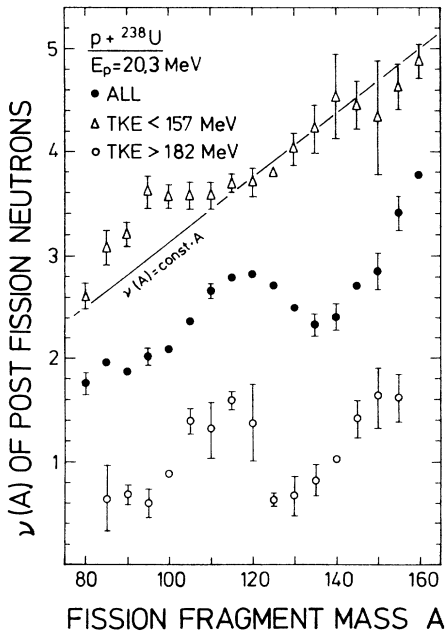

FIG. 14. Postscission neutron multiplicity per fragment for $p+^{238}U$ at $E_p=20.3$ MeV as a function of fragment mass for different ranges of the TKE.

dependence ν_{pre}(TKE) should not have an influence on it.

This result is—as were those[17] for $^{19}F+^{232}Th$ at $E_{lab}=105$ and 120 MeV—at variance with the predictions stated in the random neck rupture model; it fits well into the systematic for the difference Δn between the yield of $\nu_{post}(m)$ at the peak and the minimum in the sawtooth given in Fig. 6 of Ref. 17 indicating that the sawtooth is washed out for initial excitation energies E^*_{CN} in excess of 30–40 MeV. It might indicate, too, that the random neck rupture model in this respect becomes less correct with increasing excitation energy because, e.g., the extent of deformation changes or charged particle emission becomes more important. Statistical-model calculations show[57] that the proton multiplicities show a pronounced sawtooth structure that, with decreasing suppression by Coulomb effects, may reduce the effect in the neutron channels.

The overall slope $\Delta\text{TKE}/\Delta\nu_{post}$ amounts (Fig. 15) to 6.9 MeV/n and varies with fragmentation only to the extent the average neutron separation energy does (± 1 MeV/n). The average postscission multiplicity per fragment for events with TKE < 157 MeV (Fig. 14) is 3.6. These values represent a striking agreement with those for $p+^{238}U$ at $E_p=155$ MeV (Ref. 33), namely 7.6 MeV/n and (for TKE < 154 MeV) 3.4 neutrons. They reflect, as stated before, that the fragments only receive an increasingly less share of the additional excitation energy—in this case of about 130 MeV—due to the minimum fusion-fission timescale[3] of approximately 3×10^{-20} s.

C. Fragment temperatures

The increase with E_p of intrinsic excitation energy in the composite system ^{239}Np being accessible to the nascent fragments has been estimated with Eq. 10(b). From this result we may expect a corresponding variation of the fragment nuclear temperature T with the TKE for a

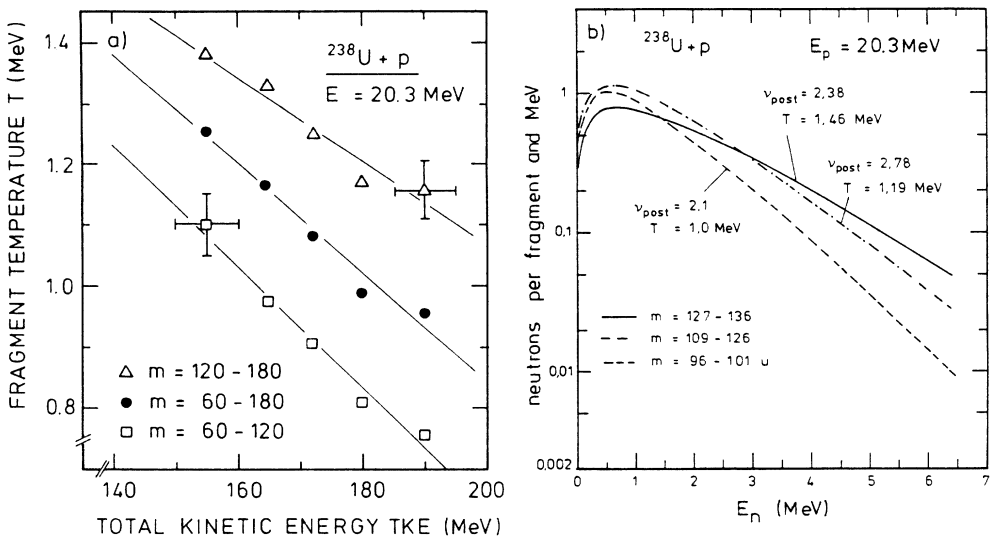

FIG. 16. (a) Fragment temperatures T from fits to postscission neutron energy spectra as a function of TKE for different fragment mass ranges. The solid lines represent linear fits. (b) Selected fits to postscission neutron energy spectra (all values of TKE, different fragment mass ranges) from the reaction system $p+^{238}$U, $E_p=20.3$ MeV.

given E_p. In addition, this dependence is anticipated in view of the results presented in Figs. 14 and 15. Indeed, Fig. 16(a) shows a linear dependence T(TKE) derived with fits of Eq. (9) to neutron energy spectra for TKE bins of approximately 10 MeV and *all* fragmentations included. The slope is $-\Delta\text{TKE}/\Delta T\approx 105$ in good confirmation of Eq. 10(b).

However, the slopes obtained in Fig. 16(a) for neutron energy spectra of the light (L) and heavy (H) fragments, respectively, differ such that $(-\Delta\text{TKE}/\Delta T)_H > (-\Delta\text{TKE}/\Delta T)_L$. In addition, the light fragments have systematically lower temperatures than the heavy ones, and Fig. 15 and 16(b) show that this difference is substantial. For an explanation the total excitation energy E_F^* of a fragment may be divided into the intrinsic part reflecting the statistical equilibrium up to the scission point, $a_F T_0^2$, and a contribution X_F resulting from the deformation of the nascent fragments,

$$E_F^*=a_F T_0^2+X_F \ . \tag{20}$$

Whereas the first term is in proportion to the fragment mass, the second one can be oversized in this respect for the heavy fragment. According to Ref. 33, this may be an outcome of the higher deformability of this fragment. In the scission point model, a spherical configuration for one fragment can only be achieved on the expense of liquid drop energy and partial compensation by a large deformation of the complementary fragment. A similar argument holds for the random rupture model.[11] It is shown in Ref. 12 for ^{236}U, that for the most probable mass split $\frac{96}{140}$ the heavy fragment is highly deformed, the light one, however, less [Fig. 5 in Ref. 12] due to the neutron shell closure for $N=88$ and $\beta_H=0.65$.

The decrease of the TKE for asymmetric mass splits with $A_H=130-140$ for $p+^{238}$U with increasing initial excitation E_{CN}^* (cf. Fig. 4) reflects (Ref. 12) an increasing deformation $(\beta_L+\beta_H)$ of both fragments which is concentrated on β_H. Similarly, for a given E_{CN}^* it leads to the additional excitation energy of the heavy fragment visible in Fig. 16(a) as $T_H-T_L>0$, because the nascent fragments snap back into a more spherical shape releasing the deformation energy for additional excitation.

With increasing internal excitation in the nascent fragments this effect, as being of shell structure origin, washes out. Accordingly the different slopes $(-\Delta\text{TKE}/\Delta T)_H > (-\Delta\text{TKE}/\Delta T)_L$, asymptotically lead to equal temperatures in the fragments and a more linear dependence $\nu_{post}\sim m$ (cf. Fig. 14). In addition, the temperature T_0 in Eq. (20) will differ by more than a factor $\frac{12}{11}$ from the fit parameter T in case of nonnegligible contributions of charged particle emission at the beginning of the evaporation cascade.

V. SUMMARY

Multiplicities, energies, and fragment correlations of fission coincident neutrons have been measured for bombardment of ^{235,236,238}U with 12.7–25.6 MeV protons. The fragments have been detected with scintillator foils or surface barrier detectors for fragment mass and (in the latter case) also energy spectroscopy.

The fragments show mass and energy distributions consistent with earlier results for the lower projectile energy range $E_p=7-13$ MeV; in particular the average TKE continues to have opposite slopes $\Delta\text{TKE}/\Delta E_p$ for symmetric and asymmetric mass splits.

The neutron spectra were unfolded into prescission and postscission contributions under the assumption of isotropic emission in the rest frames of the respective sources. The resulting multiplicities $\nu_{iso}(E_{CN}^*)$ and $\nu_{post}(E_{CN}^*)$ increase with initial excitation E_{CN}^* with comparable rates; the fusion-fission process observed is therefore slow enough to allow for this increase of ν_{iso} and at

the same time fast enough to have some of the additional excitation energy transferred into the fragments. For $p+^{238}$U at $E_p=20$ MeV it is found that the fragment TKE and their excitation energies as measured via ν_{post} (and a correction for γ emission) exhausts the total energy available.

The prescission multiplicities $\nu_{iso}(E^*_{CN})$ are incompatible with the transition-state model for energies $E^*_{CN}>20$ MeV as shown with a detailed statistical-model calculation. Beyond this excitation, the calculated time for equilibrium emission of the observed number of neutrons is $\leq 10^{-19}$ s and thus comparable with times that are attributed to a delay at the saddle-point configuration or the transition from saddle-to-scission point in heavy-ion-induced reactions with $E^*_{CN}\geq 50$ meV and fissilities $x\geq 0.70$. It is demonstrated that the inclusion of those dynamical effects in a phenomenological way does indeed improve the agreement with the experimental data. Our prescission results confirm the existing systematics in the fissility region $x\approx 0.75$ down to excitation energies $E^*_{CN}\approx 20$ MeV and the dynamic timescales deduced.

The dependence of $\nu_{post}(m)$ on fragment mass follows a sawtooth shape for $p+^{235}$U as well as for ^{238}U that washes out with increasing E_p, but is still clearly visible for $E_p=25.6$ MeV. It is shown that the heavier fragments receive for increasing E_p much more of the additional excitation energy than the light ones do. Postscission multiplicities as a function of TKE supplement these findings: The sawtooth is very much reduced for events with TKE <157 MeV. The average fragment temperatures deduced from the moving source fits are higher for the heavier fragments than for the lighter ones; they increase with decreasing TKE with their relative difference becoming smaller.

ACKNOWLEDGMENTS

The authors would like to thank Dr. H. Delagrange for making the code GIVAB available to them, Dr. Folger (Gesellschaft für Schwerionenforschung Darmstadt), and Dr. Wirth (Heidelberg) for careful preparation of some targets for this work, and Dr. W. Westmeier for the calculations with the code WEGI. They further appreciate useful discussions with Dr. U. Brosa, Dr. D. Hilscher, and Dr. D. Hinde. This work was supported by the Bundesministerium für Forschung und Technologie under Contract Nos. 06 HH 175 and 06 HH 443.

*Present address: Kernforschungszentrum Karlsruhe, IK1, D-7500 Karlsruhe 1, F.R.G.

[1]D. J. Hinde, D. Hilscher, and H. Rossner, in *Proceedings of the Symposium on Nuclear Dynamics and Nuclear Disassembly,* Dallas, Texas, 1989, edited by J. B. Natowitz (World Scientific, Singapore, 1989), p. 289.

[2]D. J. Hinde, H. Ogata, M. Tanaka, T. Shimoda, N. Takahashi, A. Shinohara, S. Wakamatsu, K. Katori, and H. Okamura, Phys. Rev. C **39**, 2268 (1989).

[3]D. Hilscher, D. J. Hinde, and H. Rossner, in *Proceedings of the Texas A&M Symposium on Hot Nuclei,* College Station, Texas, 1987, edited by S. Shlomo, R. P. Schmitt, and J. P. Natowitz (World Scientific, Singapore, 1988), p. 193.

[4]D. Hilscher, H. Rossner, B. Cramer, B. Gebauer, U. Jahnke, M. Lehmann, E. Schwinn, M. Wilpert, T. Wilpert, H. Frobeen, E. Mordhorst, and W. Scobel, Phys. Rev. Lett. **62**, 1099 (1989).

[5]C. J. Bishop, R. Vandenbosch, R. Aley, R. W. Shaw, and I. Halpern, Nucl. Phys. **A150**, 129 (1970).

[6]C. J. Bishop, I. Halpern, R. W. Shaw, and R. Vandenbosch, Nucl. Phys. **A198**, 161 (1972).

[7]D. J. Hinde, R. J. Charity, G. S. Foote, J. R. Leigh, J. O. Newton, S. Ogaza, and A. Chatterjee, Nucl. Phys. **A452**, 550 (1986).

[8]C. Gregoire, C. Ngo, E. Tomasi, B. Remand, and F. Scheuter, Nucl. Phys. **A387**, 37c (1982).

[9]Y. Patin, S. Cierjacks, J. Lachkar, J. Sigaud, G. Haouat, and F. Coçu, Nucl. Instrum. Methods **160**, 471 (1979).

[10]K. Brinkmann, J. Kiesewetter, F. M. Baumann, H. Freiesleben, H. J. Lütke-Stetzkamp, H. J. Paul, H. G. Schwenke, and H. Sohlbach, Nucl. Instrum. Methods **A276**, 557 (1989).

[11]U. Brosa, Phys. Rev. C **32**, 1438 (1985).

[12]B. D. Wilkins, E. P. Steinberg, and R. R. Chasman, Phys. Rev. C **14**, 1832 (1976).

[13]U. Brosa and S. Grossmann, Z. Phys. A **310**, 177 (1982).

[14]J. R. Nix and W. J. Swiatecki, Nucl. Phys. **71**, 1 (1965).

[15]S. Grossmann and U. Brosa, Z. Phys. A **319**, 327 (1984).

[16]D. R. Benton, H. Breuer, F. Khazaie, K. Kwiatkowski, V. E. Viola, S. Bradley, A. C. Mignerey, and A. P. Weston-Dawkes, Phys. Rev. C **38**, 1207 (1988).

[17]D. J. Hinde, J. R. Leigh, J. J. M. Bokhorst, J. O. Newton, R. L. Walsh, and J. W. Boldeman, Nucl. Phys. **A472**, 318 (1987).

[18]R. L. Ferguson, F. Plasil, F. Pleasonton, S. C. Burnett, and H. W. Schmitt, Phys. Rev. C **7**, 2510 (1973).

[19]P. Plischke, W. Scobel, and R. Wien, Nucl. Instrum. Methods **203**, 419 (1982).

[20]P. Plischke, R. Langkau, W. Scobel, and R. Wien, Nukleonika **27**, 285 (1982).

[21]K. Paasch, H. Krause, and W. Scobel, Nucl. Instrum. Methods **221**, 558 (1984).

[22]Y. Holler, A. Kaminsky, B. Scharlemann, H. Krause, R. Langkau, W. Peters, G. Poppe, N. Schirm, W. Scobel, and R. Wien, Nucl. Instrum. Methods A **235**, 123 (1985).

[23]L. C. Northcliffe and R. F. Shilling, Nucl. Data A **7**, 233 (1970).

[24]M. Strecker, Ph.D. thesis, University of Hamburg, 1990.

[25]H. W. Schmitt, W. E. Kitzer, and C. W. Williams, Phys. Rev. **137**, B837 (1965).

[26]E. Weissenberger, A. Oed, F. Gönnenwein, and H. Faust, Nucl. Instrum. Methods A **248**, 506 (1986).

[27]U. Brosa, S. Grossmann, and A. Müller, Z. Phys. A **325**, 241 (1986); Z. Naturforsch **41a**, 1341 (1986).

[28]U. Brosa and S. Grossmann, Z. Phys. A **310**, 177 (1983).

[29]V. E. Viola, K. Kwiatkowski, and M. Walker, Phys. Rev. C **31**, 1550 (1985).

[30]S. Grossmann, U. Brosa, and D. Müller, Nucl. Phys. **A481**, 340 (1988).

[31]J. R. Boyce, T. D. Hayward, R. Bass, H. W. Newton, E. G. Bilpuch, and F. O. Purser, Phys. Rev. C **10**, 231 (1974).

[32]A. Gayer and Z. Fraenkel, Phys. Rev. C **16**, 1066 (1977).

[33]E. Cheifez, Z. Fraenkel, J. Galin, M. Lefort, J. Péter, and X. Tarrago, Phys. Rev. C **2**, 256 (1970).
[34]Z. Fraenkel, I. Mayk, J. P. Unik, A. J. Gorski, and W. D. Loveland, Phys. Rev. C **12**, 1809 (1975).
[35]A. Gavron, Phys. Rev. C **13**, 2562 (1976).
[36]H. Märten and D. Seeliger, J. Phys. G **14**, 211 (1988).
[37]D. W. Lang, Nucl. Phys. **53**, 113 (1964).
[38]R. Vandenbosch and J. R. Huizenga, *Nuclear Fission* (Academic, New York, 1973).
[39]H. Nifenecker, C. Signarbieux, R. Babinet, and J. Poitou, in *Proceedings of the Third International Atomic-Energy Agency Symposium on the Physics and Chemistry of Fission,* Rochester, 1973 (IAEA, Vienna, 1974), Vol. II, p. 117.
[40]A. Gavron, Nucl. Instrum. Methods **115**, 93 (1974).
[41]P. A. Seeger and W. M. Howard, At. Data Nucl. Data Tables **17**, 428 (1976).
[42]J. Gilat, A. Fleury, H. Delagrange, and J. M. Alexander, Phys. Rev. C **16**, 694 (1977).
[43]H. Delagrange, A. Fleury, and J. M. Alexander, Phys. Rev. C **17**, 1706 (1978).
[44]B. B. Back, H. C. Britt, B. Leroux, and J. D. Garrett, Phys. Rev. C **10**, 1948 (1974).
[45]F. G. Perey, Phys. Rev. **131**, 745 (1963).
[46]A. Gavron, H. C. Britt, E. Konecny, J. Weber, and J. B. Wilhelmy, Phys. Rev. C **13**, 2374 (1976).
[47]S. Bjørnholm, A. Bohr, and B. R. Mottelson, in *Proceedings of the Third International Atomic-Energy Agency Symposium on Physics and Chemistry of Fission* (Ref. 39), Vol. I, p. 367.
[48]H. C. Britt and A. Gavron, in *Proceedings of the International Symposium on Nuclear Fission and Related Collective Phenomena and Properties of Heavy Nuclei, Bad Honnef, 1987,* Vol. 158 of *Lecture Notes in Physics,* edited by P. David, T. Mayer-Kuckuk, and A. vander Woude (Springer-Verlag, Berlin, 1981), p. 24.
[49]D. G. Madland and J. R. Nix, Nucl. Sci. Eng. **81**, 213 (1982).
[50]K. Knoche, E. Mordhorst, W. Scobel, L. Sprute, M. Strecker, B. Gebauer, D. Hilscher, M. Lehmann, H. Rossner, and T. Wilpert, *Proceedings of the International Conference on 50 Years of Research in Nuclear Fission,* Berlin, 1989, Hahn-Meitner Institut für Kernforschung Berlin GmbH Report No. B464 (Berlin, 1989), p. 74.
[51]J. O. Newton, D. J. Hinde, R. J. Charity, J. R. Leigh, J. J. M. Bokhorst, A. Chatterjee, G. S. Foote, and S. Ogaza, Nucl. Phys. **A483**, 126 (1988).
[52]P. Grange and H. A. Weidenmüller, Phys. Lett. **96B**, 26 (1980).
[53]W. Westmeier and R. A. Estlund, Z. Phys. A **316**, 27 (1984).
[54]W. Westmeier and J. Gilat (unpublished).
[55]R. Bock, Y. T. Chu, M. Dakowski, A. Gobbi, E. Grosse, A. Olmi, H. Sann, D. Schwalm, U. Lynen, W. Müller, S. Bjørnholm, H. Esbensen, W. Wölfli, and E. Morenzoni, Nucl. Phys. **A388**, 334 (1982).
[56]H. Rossner, D. Hilscher, D. J. Hinde, B. Gebauer, M. Lehmann, M. Wilpert, and E. Mordhorst, Phys. Rev. C **40**, 2629 (1989).
[57]K. Arnold, I. Düring, H. Kalka, H. Märten, A. Ruben, and D. Seeliger, Nucl. Phys. **A502**, 325C (1989).